AUTOMATIC EXTRACTION OF THE LEFT ATRIAL ANATOMY FROM MR FOR ATRIAL FIBRILLATION ABLATION

Rashed Karim, Daniel Rueckert

Imperial College London
Department of Computing
London, United Kingdom

Raad Mohiaddin, Peter Drivas

Royal Brompton Hospital
Cardiovascular and Magnetic Resonance Unit
London, United Kingdom

ABSTRACT

This paper describes and evaluates methods to detect pulmonary vein drainages and create detailed vessel trees of each drainage from contrast-enhanced magnetic resonance angiography (MRA). This description of the drainage allow us to determine the highly complex left atrial anatomy in a qualitative and quantitative way. It is beneficial for planning atrial fibrillation ablation procedures. We conclude that our methods permit the creation of drainage trees for the detailed description of the atrial anatomy from cardiac MRA data.

Index Terms— Segmentation, magnetic resonance angiocardiography, Blood vessels

1. INTRODUCTION

There is a growing interest in quantifying the precise anatomy of the human heart before surgical interventions. Atrial fibrillation (AFib) is the most common superventricular arrhythmia with significant morbidity and mortality. It is also now well established that the anatomical architecture of the left atrium and pulmonary veins (PV) play an important role in the genesis and maintenance of AFib [1].

Traditional techniques used in electrophysiology can accurately map electrical activity in the atrial chambers but cannot resolve the underlying left atrial anatomy. The anatomy of the left atrium is highly complex and shows significant inter-subject variability [1]. Understanding its anatomy is important for the successful restoration of normal sinus rhythm in AFib patients [2]. The use of contrast enhanced MRA for obtaining the detailed 3D anatomy of the left atrium has thus gained great importance in AFib corrective procedures. It is desirable to visualize the left atrial anatomy without the interference of neighbouring blood vessels and chambers. There is little known work on left atrium segmentation, except for the work in [3, 4].

2. LEFT ATRIUM AND ATRIAL BODY SEGMENTATION

The images acquired for this study are contrast-enhanced MRA images. The left atrium (LA) is segmented using a segmentation method, previously described in [5]. In this paper, the LA refers to the atrium and also includes the pulmonary veins that drain into it. The segmented LA contains voxels that belong to two sub-atrial structures: 1) central atrial body, and 2) pulmonary veins. The segmentation of the atrial body is desirable, before determining the PV. The method is based on evolving surfaces using level set methods with two consecutive evolution processes, each under a different speed function derived from the sigmoid:

$$S(x) = \frac{1}{1 + e^{-(\frac{x-\beta}{\alpha})}} \tag{1}$$

where α, β are scaling parameters of the sigmoid. The first evolution step obtains an approximation of the atrial body shape. This approximation is improved in the second evolution step. The first evolution is influenced by the speed function $S(d)$ where d is the Euclidean distance value. Here, the distance values are from the Euclidean distance (ED) transformation of the *binary* segmented atrium image. The second evolution is influenced by the speed function $S(\nabla I)$ where ∇I is the image gradient. In this step, the approximate shape obtained in the first step is used as the initial surface. A curvature constraint imposed on the evolving surface, in the second evolution step, prevents leaks through the LA-PV junction by preventing large deviances from the initial approximated shape.

3. PULMONARY VEIN CENTERLINES

The PV centerline extraction process is based on determining the medial axis of tubular structures. This is found by maximizing the ED transform function of the binary segmented LA image. The ED transform is computed on the segmented atrium image using a fast and exact method described in [6].

3.1. Determining vessel direction

Prior to centerline tracking, vessel directions at each voxel location are determined. The directions are found by analyzing the second-derivative information or Hessian H of the Gaussian smoothed image containing vessels [7]. It is assumed that there is a good contrast between vessel and background. With Gaussian smoothing, minimum intensity variation is expected to be found in the vessel direction. Maximum intensity variations are found in the two directions orthogonal to the vessel axis. An eigen decomposition of the Hessian give the amount of intensity variations and their directions. Let $\lambda_1, \lambda_2, \lambda_3$ be ordered eigenvalues of H with $|\lambda_1| \leq |\lambda_2| \leq |\lambda_3|$ and $\mathbf{v}_1, \mathbf{v}_2, \mathbf{v}_3$ as corresponding eigenvectors. The vessel direction is then given by $\mathbf{v}_1$. As vessels vary in diameter, a multi-scale approach is used with smoothing applied only at selected scales. Vessel directions are thus extracted at scales that match the vessel diameter. The correct scales are determined using a vessel response filter [7].

3.2. Automatic seed selection

With the atrial body segmented and subtracted from segmented LA, most voxels that remain are PV. To track PV centerlines, seed points within vessels from which the tracking process can initiate are generated. It is desirable to generate seeds only within the vessels but not the atrial body. A vesselness filter [7] produces high responses in voxels within vessels. Using this filter, voxels that have a vesselness filter response higher than a certain threshold value are used as seeds, ensuring only tubular structures are explored. We randomly select 5% of total voxels with high response. This normally generates between 1000-5000 seed points.

3.3. Centerline tracking

Centerline tracking is an iterative process, where at each step the ED transform function ξ of the segmented LA is maximized. This works on the principle that the medial axis can be reconstructed by finding local maximums of the ED function at vessel planes, and connecting these with an approximating spline. The process makes progress by moving forward along the vessel, i.e. a small number of steps in the vessel direction $\mathbf{v}_1$. The process is repeated at this newly arrived point. Fig. 1 illustrates the tracking process.

At each iterative step, the distance function ξ is maximized along the plane Γ, which is perpendicular to the vessel direction $\mathbf{v}_1$ and passes through the seed point $\mathbf{s}$:

$$\Gamma : \mathbf{v}_1 \cdot (\mathbf{x} - \mathbf{s}) = 0 \tag{2}$$

By constraining the maximization to this plane, repeated convergences to a same local maximum of ξ, due to its catchment basin, is avoided. Maximization is accomplished using a hill-climbing approach. Starting from a seed $\mathbf{s}$, the direction of maximum ascent is followed by exploring its 8-neighborhood. These neighbour locations are found by interpolating them on the plane Γ.

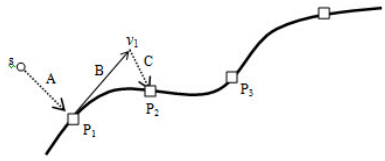

Fig. 1. **A** - Starting from a seed point s, the ED transform ξ is maximized, bringing us to a centerline point P_1. **B** - A small number of steps is taken in the vessel direction $\mathbf{v}_1$. **C** - The function ξ is maximized again yielding a new centerline P_2.

Termination conditions are imposed for allowing the tracking process to stop. When the vessel tracker is outside the vessel, or inside the atrial body, the tracking process is stopped. In addition to this the tracking is also stopped if the degree of curvature between consecutive centerline points becomes too large.

4. TREE REPRESENTATION OF THE PULMONARY VEINS

Centerline tracking produces disconnected segments and it is useful to connect them in some ordered fashion. This also helps construct a tree-like representation of the PV. Two important steps in building the vessel tree are discussed: 1) Finding the root vessels for each tree and, 2) the cost function for establishing parent-child connections.

4.1. Finding PV drainage and root vessels

Prior to computing the PV trees, centerline segments close to the atrial body are found. Some of these are centerlines of PV drainages to the atrial body and ideal candidates for root of PV trees. A simple and fast technique is proposed to find these drainages. Distances between the centerline endpoints and atrial body surface are computed. Assume two subsets in the image space I: left atrium (LA) and atrial body (AB) where $AB \subset LA \subset I$:

$$\overline{AB} = I \backslash AB \tag{3}$$

Let $\xi(.)$ denote the ED transform operator on a binary image. We can thus compute $\xi(\overline{AB})$ which gives the shortest distance value of each voxel to the atrial body surface. Centerline segment endpoints with distance values less than τ in $\xi(\overline{AB})$ are selected.

To handle these cases and to ensure only a single segment is selected as the root to represent the drainage tree, we use a hierarchical clustering algorithm [8] to group centerline segments C. The closest endpoint, to the atrial body surface, of each centerline segment in C is used as the data for clustering. Since, drainages are spatially located on both the left and right

sides of the atrial body, a variance measure on the inter-cluster distances can be used to identify the optimal cluster grouping. Once clusters are identified, a centerline segment from each cluster is selected as the root vessel for that drainage, preferably the one with the largest length.

4.2. Parent-child connections

With a root vessel centerline segment selected, child nodes are progressively attached to the connected base, by evaluating the cost of connection with a cost function. These attachments are straight lines connecting the child to the parent. A possible connection is supported by two criteria: 1) the shortest distance between the parent and child vessel segment, and 2) the average vesselness filter response along the straight line drawn for the re-connection. A cost function $c : \mathbb{R} \rightarrow [-1, 1]$ examines these criteria for evidence of a connection:

$$c = \omega\mathcal{V} + (1 - \omega)\mathcal{D} \tag{4}$$

where $\omega \in [0, 1]$, trades off penalty function for vesselness measure $\mathcal{V}$ and for the spatial proximity $\mathcal{D}$. The penalty functions $\mathcal{V}$ and $\mathcal{D}$, are derived from the sigmoid which clamp penalty values between $[-1, 1]$, where positive penalty favors connection and negative penalty otherwise.

The penalty term for spatial proximity is straightforward: Any parent-child connection distance is penalized according to their distance d:

$$\mathcal{D} = 1 - \frac{2}{1 + e^{-(d-\epsilon)}} \tag{5}$$

where any distance greater than ϵ acquires negative penalty. For our purposes we use $\epsilon = 6$. The penalty function $\mathcal{V}$ for the vesselness measure is based on the observed distribution of vesselness filter responses over all detected centerline segments. We assume that the vesselness measure over the detected centerlines is normally distributed: $N(\mu, \sigma)$ with mean μ and variance σ^2. The average vesselness measure μ_0 along the proposed parent-child connection is determined and a negative penalty is assigned if its z-score is less than -κ, i.e. $\mu_0 < -\kappa\sigma$. We use $\kappa = 2$. Since high vesselness is a strong indicator of vessel connection, a positive penalty is assigned not only when $\mu_0 \geq -\kappa\sigma$, but also when $\mu_0 > +\kappa\sigma$. This is achieved using:

$$\mathcal{V} = \frac{2}{1 + e^{-(z+\kappa)}} - 1, \text{ where } z = \frac{\mu_o - \mu}{\sigma} \tag{6}$$

Given a potential parent-child connection, the cost function in eq. 4 is evaluated for every pair of sampled points on the parent and child centerline segments, with a straight line drawn between them. A positive cost value indicates a connection.

5. LEFT ATRIAL ANATOMY

Using the constructed PV drainage trees, the left atrial anatomy can now be classified. The number of drainages to each side of the atrium including the first bifurcation distances help classify the anatomy according to [1]. The first bifurcation distance for each tree is computed using geodesic distances between first child and root nodes. Diagrammatic representations of the underlying trees are also generated showing its configurations for each drainage (see Fig. 3).

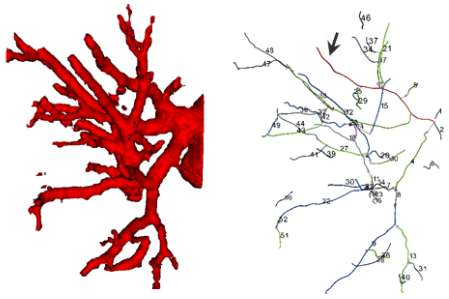

Fig. 2. Surface reconstruction of a PV drainage (left). The detected and annotated centerlines; vessels are annotated using numbers by the system for easy reference (right). The root node vessel is indicated by the arrow.

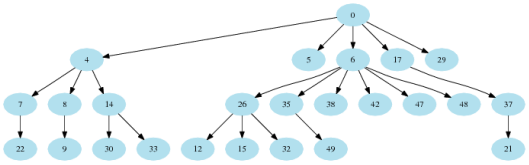

Fig. 3. The extracted vessel tree from drainage in Fig. 2

6. RESULTS

The data acquired are MR angiography studies of 30 different patients. The images have in-plane resolutions ranging between 250×350 to 380×380. Each image volume contains between 30-100 slices. There was significant amount of anatomic variability of the left atrium between patient subjects. The studies contained pre- and post-MRA scans which were registered using rigid registration. An anisotropic diffusion smoothing step was used to remove noise and preserve edges.

For evaluating atrial anatomy, two important determinants of anatomy are qualitatively evaluated against ground truth. These are first bifurcation distances and the number of drainages to the right and left sides of the atrium. The atrial classification system proposed in [1] uses these features to identify anatomy. For the first bifurcation distance study, the percentage error in the computed values were found by comparing them against ground truth. Ground truth was obtained from surface reconstructed images of the LA. Note also that distances were evaluated for each PV drainage of the 30 atria studied. 41% of the drainages studied had an error in first

bifurcation distances of less than 15%. This is illustrated in Fig. 7. For evaluating the number of drainages found to each side of the atrium, computed values were compared against ground truth. These are illustrated in Fig. 5 and 6 for the left and right sides respectively. A success rate of 87% and 93% was found for left and right sides respectively.

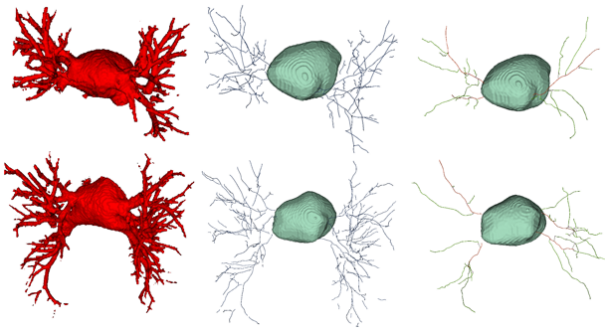

Fig. 4. Surface reconstructions of two segmented left atria (left column). The segmented atrial bodies along with all the detected PV centerlines (middle column). Only detected drainage trees, with higher tree levels truncated (right column)

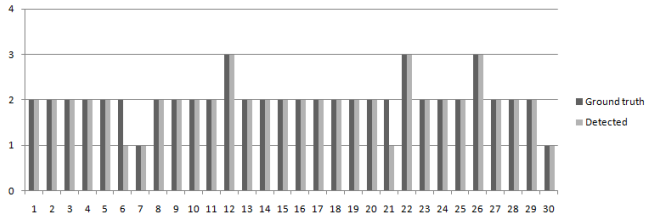

Fig. 5. Comparisons of the number of drainages to the left side of 30 patient atria.

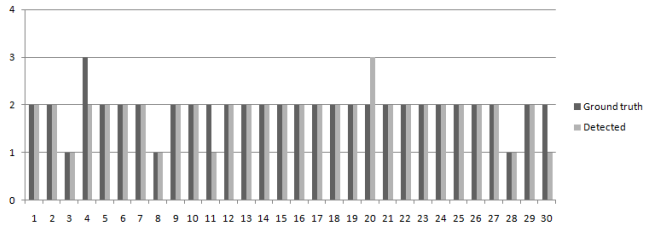

Fig. 6. Comparisons of the number of drainages to the right side of 30 patient atria.

7. DISCUSSION

Results indicate that this is a robust technique for extracting and reporting left atrial anatomy. The centerline detection, tree building process and computation of bifurcation distances are fast requiring less than 10 seconds on a modern PC. It also requires no special imaging acquisition and has been shown to work on MRA data. The tree representation of the drainages determines the anatomy and also makes it possible to truncate peripheral vessels of the drainage (i.e. at higher levels down in the tree), giving a less obstructed view of the atrium. These are very beneficial for atrial fibrillation ablation procedures.

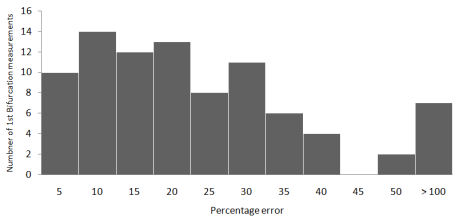

Fig. 7. Percentage errors in the computed first bifurcation distances in 116 drainages studied.

8. REFERENCES

[1] E.M. Marom, J.E. Herndon, Y.H. Kim, and H.P. McAdams, "Variations in Pulmonary Venous Drainage to the Left Atrium," *Radiology*, p. 230303031, 2004.

[2] R. Kato, L. Lickfett, Meininger, and et al., "Pulmonary Vein Anatomy in Patients Undergoing Catheter Ablation of Atrial Fibrillation," *Circ.*, vol. 107, no. 15, pp. 2004, 2003.

[3] A. Cristoforetti, L. Faes, Ravelli, and et al., "Isolation of the left atrial surface from cardiac multi-detector CT images based on marker controlled watershed segmentation," *Med Eng and Physics*, vol. 30, no. 1, pp. 48–58, 2008.

[4] M. John and N. Rahn, "Automatic Left Atrium Segmentation by Cutting the Blood Pool at Narrowings," *Lec Notes in Comp Sci*, vol. 3750, pp. 798, 2005.

[5] R. Karim, R. Mohiaddin, and D. Rueckert, "Left atrium segmentation for atrial fibrillation ablation," 2008, vol. 6918, p. 69182U, SPIE.

[6] T. Saito and J.I. Toriwaki, "New algorithms for euclidean distance transformation of an n-dimensional digitized picture with applications," *Pattern Recognition*, vol. 27, no. 11, pp. 1551–1565, 1994.

[7] A.F. Frangi, W.J. Niessen, K.L. Vincken, and M.A. Viergever, "Multiscale Vessel Enhancement Filtering," *Lec Notes in Comp Sci*, pp. 130–137, 1998.

[8] S.C. Johnson, "Hierarchical clustering schemes," *Psychometrika*, vol. 32, no. 3, pp. 241–254, 1967.